ASME Journal of Applied Mechanics
Online journal at:
https://asmedigitalcollection.asme.org/appliedmechanics

Analytical Solutions for Circular Elastic Membranes Under Pressure

Zhaohe Dai
Department of Mechanics and Engineering Science,
State Key Laboratory for Turbulence and Complex Systems,
College of Engineering,
Peking University,
Beijing 100871, China
e-mail: daizh@pku.edu.cn

This study investigates the problem of a circular elastic membrane clamped or adhered at its boundary and subjected to uniform transverse pressure. Many analytical solutions for this classical problem have been developed previously, using either a series-based approach (notably accurate but lengthy and implicit) or approximate kinematics (relatively simple yet lacking accuracy). Here, we seek new analytical solutions using a perturbed spherical cap to represent the shape of the pressurized membrane. Our approach yields simple, explicit solutions of remarkable accuracy for the deformed profile, pressure–deflection relation, strain distributions, and energy release rate, which are directly applicable to emerging ultrathin membrane systems. [DOI: 10.1115/1.4065338]

Keywords: membranes, blister tests, large deflection, thin films, 2D materials, elasticity, energy release rate and delamination, structures

1 Introduction

The widespread use of circular elastic membranes across various applications, including blister tests, pressure sensors, field-effect transistors, and lightweight structures [1–5], has sparked significant interest in pressure-loaded or pressurized circular membranes. Specifically, there is considerable focus on a scenario where the deformed geometry demonstrates large deflection alongside moderate rotation [2,3,6]. The large deflection (relative to the membrane thickness) allows the plate bending to be ignored, while the moderate rotation allows the use of linear material laws. In this context, the Föppl membrane theory, or the membrane limit of the Föppl-von Kármán equations, is commonly employed to characterize the mechanical response of pressurized membranes [7–11]. Despite its apparent simplicity, the involvement of nonlinear kinematics in solving this set of equations poses challenges. As a result, existing analytical solutions in literature often tend to be either implicit and lengthy [7,12,13] or prone to accuracy issues [2,14–17] (which will be detailed shortly). In this work, the objective is to derive analytical solutions that offer both simplicity and accuracy. We demonstrate that achieving this is possible simply by utilizing a perturbed spherical cap to represent the shape of pressurized membranes.

2 The Problem

Figure 1 shows the schematics of the problem of pressurized circular elastic membranes. With axisymmetry, we can write the governing equations in terms of displacements [3,19], which include the in-plane equilibrium equation:

$$\frac{\mathrm{d}^2u}{\mathrm{d}r^2}+\frac{\mathrm{d}u}{r\mathrm{d}r}-\frac{u}{r^2}+\frac{1-\nu}{2r}\left(\frac{\mathrm{d}w}{\mathrm{d}r}\right)^2+\frac{\mathrm{d}w}{\mathrm{d}r}\frac{\mathrm{d}^2w}{\mathrm{d}r^2}=0 \tag{1}$$

and the out-of-plane equilibrium equation:

$$\frac{Et}{1-\nu^2}\frac{\mathrm{d}w}{\mathrm{d}r}\left[\frac{\mathrm{d}u}{\mathrm{d}r}+\nu\frac{u}{r}+\frac{1}{2}\left(\frac{\mathrm{d}w}{\mathrm{d}r}\right)^2\right]+\frac{1}{2}pr=0 \tag{2}$$

Here, u and w denote the displacements in-plane and out-of-plane, respectively. E, t, and ν represent Young's modulus, thickness, and Poisson's ratio of the membrane, while p is the applied pressure. Solving the problem with a pinned edge at $r=a$ can be readily achieved numerically by incorporating boundary conditions such as $u(0)=w'(0)=u(a)=0$. In the case where the edge of the membrane is unpinned (as depicted in the right panel of Fig. 1), the solution involves the determination of the edge radius. Here, we apply Griffith's criterion $G=G_c$, where G is the energy release rate and G_c represents the critical energy release rate associated with the delamination of the membrane from the substrate [20,21]. For the sake of simplicity, we overlook mode mixity at the interface and assume a constant membrane–substrate adhesion ($G_c=\Gamma$) [5,22].

Analytical relations for this problem are of significant practical importance. For example, a cubic pressure–deflection relation has been extensively discussed [2,14–16,23–25], represented by:

$$p=\zeta(\nu)Et\frac{h^3}{a^4} \tag{3}$$

where h denotes the pressurized height at $r=0$, and the prefactor ζ is dependent solely on Poisson's ratio. In addition, the strain components in pressurized membranes are found to be proportional to the square of the aspect ratio [2,9,15], a factor used in strain engineering for 2D materials [4,6,26–28]. In particular, the equal biaxial strain at the membrane center can be expressed as follows:

$$\epsilon_0=\psi(\nu)\frac{h^2}{a^2} \tag{4}$$

Contributed by the Applied Mechanics Division of ASME for publication in the Journal of Applied Mechanics. Manuscript received January 26, 2024; final manuscript received April 1, 2024; published online May 7, 2024. Assoc. Editor: Jian Wu.

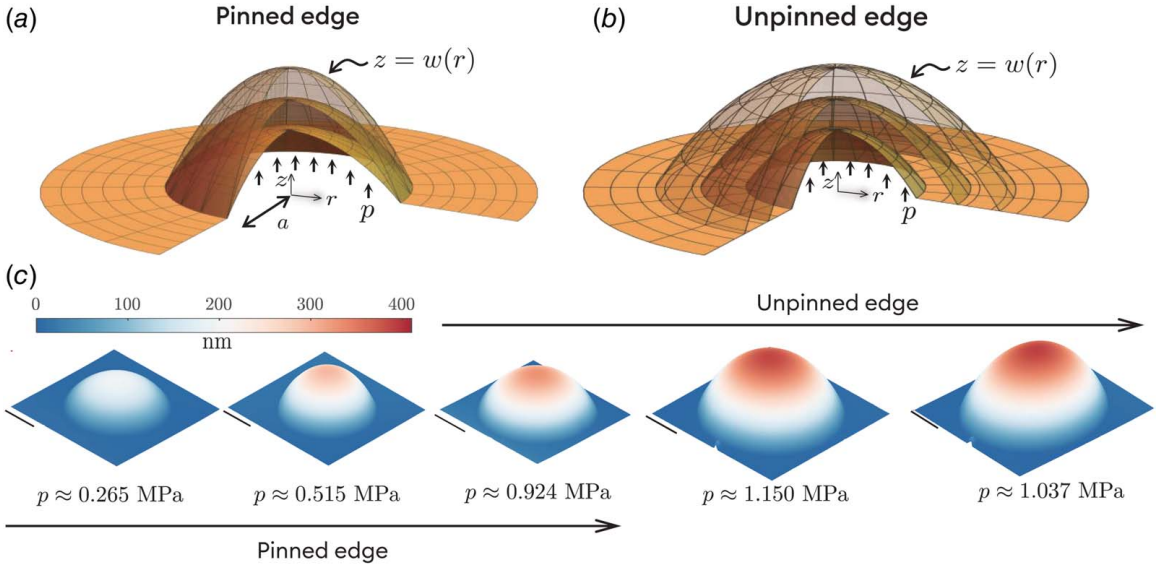

Fig. 1 Schematics of circular membranes clamped (*a*) and adhered (*b*) at the boundary. The focus is on the mechanical response of the elastic membrane under pressure loads, including the pressure–deflection relation, strain distributions, and the energy release rate when the membrane edge is allowed to delaminate from its adhered substrate. (c) Experimentally measured profiles of pressurized single-layer graphene membranes (data associated with Refs. [16,18]). The graphene is pressurized by a given amount of gas molecules with increasing height. The edge is first fixed (pinned) and then unpinned due to the delamination between the membrane and its substrate. Scale bars: 2 μm.

where ψ is a constant. In scenarios where the edge of the membrane is allowed to delaminate from the substrate under a volume-controlled condition [10,16,29–31], the height and radius of the membrane are not independent. The interplay between elastic and adhesive forces has been observed to result in a constant aspect ratio (as depicted in Fig. 1(*b*)). This relationship can be represented as follows:

$$\Gamma = \phi(\nu) E t \frac{h^4}{a^4} \tag{5}$$

where ϕ is a constant. Alternatively, in pressure-controlled setups such as blister tests, significant attention has been devoted to the critical pressure required for the blow-off of the membrane [12,23]

$$G_c = \left[\varphi(\nu)\frac{p_c^4 a^4}{Et}\right]^{1/3} \tag{6}$$

where φ is constant. Apparently, $\varphi = \phi^3/\zeta^4$.

As summarized in Table 1, there have been roughly two primary analytical approaches directed toward determining the prefactors in Eqs. (3)–(6). One approach stems from Hencky's series solution to the nonlinear problem of pinned membrane edges [7,13]. Hencky's solution comprises seven terms addressing the out-of-plane deformation and the radial stress, given by:

$$w \sim \sum_{n=0}^{7} a_{2n}\left(1 - r^{2n+2}\right) \quad \text{and} \quad N_{rr} \sim \sum_{n=0}^{7} b_{2n} r^{2n} \tag{7}$$

Constants a_{2n} and b_{2n} can be explicitly interconnected through equilibrium equations and boundary conditions, whereas the determination of b_0 requires solving an implicit characteristic equation [7,13]. As a result, prefactors in Eqs. (3)–(6) are often calculated for specific Poisson's ratios [12,14,18,23,29,30,33,34]. An alternative approach presumed either a spherical cap configuration for the pressurized membrane or constant stresses within the membrane (essentially equivalent to assuming a spherical cap shape) [2,15,16,23]:

Table 1 A summary of the methods and assumptions involved in previous analytical solutions to the pressurized elastic membrane problem

Reference	Methodology	Assumption
Hencky [7]	Equilibrium equations	Variables in a series form of seven terms
Gent and Lewandowski [12]	Hencky's solution	Specific Poisson's ratios
Wan and Mai [29]	Hencky's solution	Specific Poisson's ratios
Fichter [13]	Equilibrium equations	Variables in a series form of ten terms
Williams [23]	Equilibrium equations	Constant stresses
Wan and Lim [32]	Equilibrium equations	Constant stresses
Freund and Suresh [2]	Energy approach	Spherical cap shape and simplified displacement
Koenig et al. [30]	Hencky's solution	Specific Poisson's ratios
Yue et al. [15]	Energy approach	Spherical cap shape and simplified displacement
Sanchez et al. [33]	Energy approach	Spherical cap shape and simplified displacement
Dai et al. [16]	Equili equations	Spherical cap shape
Blundo et al. [25]	Equilibrium equations	Similar to solution I
Solution I (this work)	Equilibrium + energy approach	Perturbed spherical cap shape
Solution II (this work)	Equilibrium + energy approach	Perturbed spherical cap shape
Solution III (this work)	Equilibrium + energy approach	Perturbed spherical cap shape

Note: These models are valid for membranes of no residual stress, vanishing bending stiffness, and moderate rotation.

$$\frac{w}{h} = 1 - \left(\frac{r}{a}\right)^2 \tag{8}$$

Utilizing this, together with an energy-based method, yields straightforward explicit expressions for the prefactors as functions of Poisson's ratio, which, unfortunately, are susceptible to reduced accuracy [33]. In the subsequent section, we provide analytical solutions for the prefactors that can be presented in simple, explicit forms and, at the same time, offer an accuracy level comparable to Hencky's series solution. The analytical results will be compared with the numerical results of Eqs. (1) and (2), which are solved by discretizing the domain into finite difference grids and using a Newton–Raphson method with successive overrelaxation [19,24].

3 Analytical Approach and Results

The crux of our analytical approach lies in the shape of the pressurized membrane. The observation from numerics in Fig. 2 is that this shape deviates slightly from that of a spherical cap. We then look for minor adjustments, specifically the following three variations:

$$\frac{w(r)}{h} \sim \begin{cases} \left[1 - \left(\frac{r}{a}\right)^{2+\alpha}\right] \\ \left[1 - \left(\frac{r}{a}\right)^{2}\right]^{\beta} \\ \frac{1}{1+\varepsilon}\left[1 - \left(\frac{r}{a}\right)^{2}\right] + \frac{\varepsilon}{1+\varepsilon}\left[1 - \left(\frac{r}{a}\right)^{N}\right] \end{cases} \tag{9}$$

with $|\alpha(\nu)|$, $|\beta(\nu) - 1|$, $|\varepsilon(\nu)| \ll 1$, and $N(\nu) > 1$ (to avoid stress singularity at the origin). To solve the in-plane displacement $u(r)$, we directly use the in-plane equilibrium equation (1), rather than assuming a kinematically admissible in-plane displacement field that would introduce more unknown constants.

We can then obtain the strain fields according to the kinematics

$$\epsilon_{rr} = \frac{\mathrm{d}u}{\mathrm{d}r} \quad \text{and} \quad \epsilon_{\theta\theta} = \frac{u}{r} \tag{10}$$

and the stress fields according to Hooke's law

$$N_{rr} = \frac{Et}{1-\nu^2}(\epsilon_{rr} + \nu\epsilon_{\theta\theta}) \quad \text{and} \quad N_{\theta\theta} = \frac{Et}{1-\nu^2}(\epsilon_{\theta\theta} + \nu\epsilon_{rr}) \tag{11}$$

We use an energy method to determine the unknown constants in Eq. (9). Specifically, the total energy of the system can be written as follows:

$$\mathcal{F} = 2\pi\int_0^a \left(\frac{1}{2}N_{rr}\epsilon_r + \frac{1}{2}N_{\theta\theta}\epsilon_{\theta\theta}\right) r\,\mathrm{d}r - pV + \pi a^2\Gamma \tag{12}$$

where the volume of the pressurized membrane is

$$V = 2\pi\int_0^a wr\,\mathrm{d}r \tag{13}$$

We first calculate the prefactor for the pressure–deflection relation in Eq. (3) and the strain magnitude at the center of the membrane in Eq. (4). This can be achieved by minimizing the total energy with a pinned membrane edge, i.e.,

$$\left.\frac{\partial\mathcal{F}}{\partial h}\right|_a = 0 \quad \text{and} \quad \left.\frac{\partial\mathcal{F}}{\partial c}\right|_a = 0 \tag{14}$$

where c is the parameter α, β, or ϵ and N depending on which variation in Eq. (9) is used. To calculate the prefactor for the adhesion–strain energy relation in Eq. (5) or the critical energy release rate in Eq. (6), we focus on a displacement-controlled situation (particularly loaded by an incompressible liquid [35]) with a no-pinning condition, i.e.,

$$\left.\frac{\partial\mathcal{F}}{\partial a}\right|_V = 0 \tag{15}$$

Equations (9)–(15) complete the process of our analytical approach.

3.1 Solution I. We begin by trying the first variation of the shape of the pressurized membrane in Eq. (9), i.e.,

$$w(r) = h\left[1 - \left(\frac{r}{a}\right)^{2+\alpha}\right] \tag{16}$$

The corresponding volume is

$$V = \frac{2+\alpha}{4+\alpha}\pi a^2 h \tag{17}$$

Using the in-plane equilibrium Eq. (1) and the kinematic relations in Eq. (10) can give:

$$\epsilon_{rr} = \psi(\alpha,\nu)\frac{h^2}{a^2}\left[1 - \frac{1-(3+2\alpha)\nu}{3+2\alpha-\nu}\left(\frac{r}{a}\right)^{2+2\alpha}\right] \tag{18a}$$

$$\epsilon_{\theta\theta} = \psi(\alpha,\nu)\frac{h^2}{a^2}\left[1 - \left(\frac{r}{a}\right)^{2+2\alpha}\right] \tag{18b}$$

where

$$\psi(\alpha,\nu) = \frac{(2+\alpha)(3+2\alpha-\nu)}{8(1+\alpha)} \tag{19}$$

Now the total energy of the system can be rewritten in terms of h, a, and α as follows:

$$\mathcal{F}(\alpha,h,a) = \frac{\pi(2+\alpha)^2(7+4\alpha-\nu)}{32(3+2\alpha)(1-\nu)}Et\frac{h^4}{a^2} - \frac{2+\alpha}{4+\alpha}\pi pa^2h + \pi a^2\Gamma \tag{20}$$

For a fixed a, the minimization of the total energy with respect to h leads to $p = \zeta(\alpha,\nu)Eth^3/a^4$ with

$$\zeta(\alpha,\nu) = \frac{(2+\alpha)(4+\alpha)(7+4\alpha-\nu)}{8(3+2\alpha)(1-\nu)} \tag{21}$$

Alternatively, the minimization with respect to α gives

$$\alpha(\nu) \approx \frac{\sqrt{1025 - 742\nu + 41\nu^2} - 15 - 3\nu}{50 - 2\nu} \tag{22}$$

where we have dropped terms of the order of α^3 in calculations. Finally, for membranes with unpinned, adhesive edges subject to volume-controlled loads, the total energy reads

$$\mathcal{F}(a,V) = \frac{(4+\alpha)^4(7+4\alpha-\nu)}{32\pi^3(2+\alpha)^2(3+2\alpha)(1-\nu)}\frac{EtV^4}{a^{10}} + \pi a^2\Gamma \tag{23}$$

It is clear that the elastic energy favors large a, while the adhesion favors small a. The competition leads to $\Gamma = \phi(\alpha,\nu)Eth^4/a^4$ with

$$\phi(\alpha,\nu) = \frac{5(2+\alpha)^2(7+4\alpha-\nu)}{32(3+2\alpha)(1-\nu)} \tag{24}$$

These results based on Eq. (16) will be referred to as "solution I" and compared against other solutions.

3.2 Solution II. We move on to derive solution II using the second variation in Eq. (9), i.e.,

$$w(r) = h\left[1 - \left(\frac{r}{a}\right)^2\right]^{\beta} \tag{25}$$

Following similar steps in the preceding subsection, we can readily obtain the volume

$$V = \frac{\pi}{1+\beta}a^2h \tag{26}$$

the strain fields

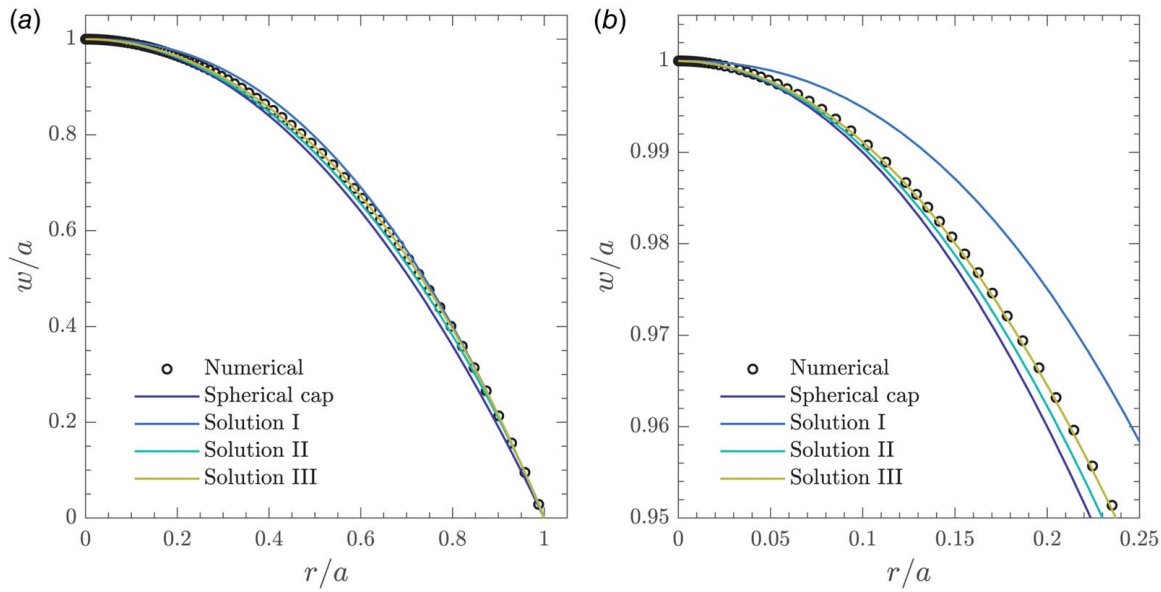

Fig. 2 **(*a*) Shape of the pressurized membrane and (*b*) its zoom-in view. The markers are obtained by numerically solving the problem (1) and (2). The expressions for the spherical cap, solution I, solution II, and solution III are given in Eqs. (8), (16), (25), and (32), respectively, where the parameters depending on Poisson's ratio are solved in Eqs. (22), (31), and (38), respectively. Here, $\nu = 0$.**

$$\epsilon_{rr} = \psi(\beta,\nu)\frac{h^2}{a^2}\frac{\left[-(1+\nu)+\left(1+\nu-4\beta\nu\right)r^2/a^2\right](1-r^2/a^2)^{2\beta-1}+(1+\nu)(1+r^2/a^2)}{[2\beta(1-\nu)+1+\nu]r^2/a^2} \tag{27a}$$

$$\epsilon_{\theta\theta} = \psi(\beta,\nu)\frac{h^2}{a^2}\frac{\left[1+\nu+(4\beta-1-\nu)r^2/a^2\right](1-r^2/a^2)^{2\beta-1}-(1+\nu)(1-r^2/a^2)}{[2\beta(1-\nu)+1+\nu]r^2/a^2} \tag{27b}$$

as well as the three prefactors including

$$\psi(\beta,\nu) = \frac{2(1-\nu)\beta^2+(1+\nu)\beta}{8\beta-4} \tag{28}$$

$$\zeta(\beta,\nu) = \frac{1}{2}(1+\beta)\beta^2\left[\frac{1}{4\beta-1}+\frac{2}{(1-\nu)(1-2\beta)^2}\right] \tag{29}$$

$$\phi(\beta,\nu) = \frac{5}{8}\beta^2\left[\frac{1}{4\beta-1}+\frac{2}{(1-\nu)(1-2\beta)^2}\right] \tag{30}$$

where

$$\beta(\nu) \approx \frac{\sqrt{7625+3026\nu-2551\nu^2}+907-373\nu}{1064-440\nu} \tag{31}$$

3.3 Solution III. We find that solutions based on the first two perturbed spherical cap shapes fail to deliver satisfactory outcomes. This can also be seen from Fig. 2, showing the disparity between the perturbed shapes generated by Eqs. (16) and (25) and the corresponding numerical results of the nonlinear problem (1) and (2) (calculated using a regular finite difference method). We then delve into solution III, which is based on the third variation outlined in Eq. (9). We use $R = r/a$ to rewrite the solution as follows:

$$w(r) = \frac{h}{1+\varepsilon}\left[\left(1-R^2\right)+\varepsilon\left(1-R^N\right)\right] \tag{32}$$

The selection of the parameter N here requires careful consideration. While it seems intuitive to opt for $N = 4$, 6, 8, and so forth, our analysis reveals that the resultant accuracy does not exhibit significant improvements over solutions I and II. Furthermore, our attempts to refine the solution by employing an expression such as $w \sim (1-R^2)+\varepsilon(1-R^4)+\varepsilon^2(1-R^6)$ only led to lengthy expressions without yielding significant advantages over Hencky's series solution. Intriguingly, setting

$$N = 5$$

resolves this issue. In this context, the volume of the pressurized membrane becomes:

$$V = \frac{7+10\epsilon}{14(1+\varepsilon)}\pi a^2 h \tag{33}$$

and the strain fields can be given by:

$$\epsilon_{rr} = \frac{f(\varepsilon,\nu)-56(1-3\nu)R^2-64(1-6\nu)R^5\varepsilon-35(1-9\nu)R^8\varepsilon^2}{224(1+\varepsilon)^2} \tag{34a}$$

$$\epsilon_{\theta\theta} = \frac{f(\varepsilon,\nu)-56(3-\nu)R^2-64(6-\nu)R^5\varepsilon-35(9-\nu)R^8\varepsilon^2}{224(1+\varepsilon)^2} \tag{34b}$$

where $f(\varepsilon,\nu) = 56(3-\nu)+64(6-\nu)\varepsilon+35(9-\nu)\varepsilon^2$. The prefactors specified in Eqs. (3)–(6) can then be derived:

$$\psi(\varepsilon,\nu) = \frac{56(3-\nu)+64(6-\nu)\varepsilon+35(9-\nu)\varepsilon^2}{224(1+\varepsilon)^2} \tag{35}$$

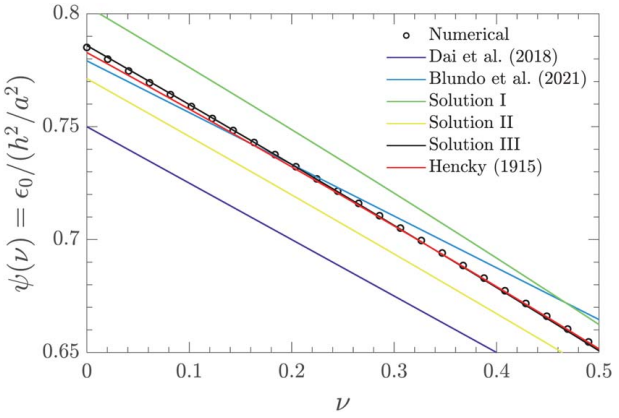

Fig. 3 The rescaled strain at the center of the pressurized membrane (i.e., ψ in Eq. (4)) as a function of Poisson's ratio. The analytical expressions of solutions I, II, and III are given in Eqs. (19), (28), and (35), respectively. The solution by Dai et al. and Blundo et al. can be found in Refs. [16] and [25], respectively. Hencky's solution is derived based on the corrected calculation outlined in Ref. [13].

$$\zeta(\varepsilon, \nu) = \frac{7-\nu}{3(1-\nu)} + \frac{149+13\nu}{63(1-\nu)}\varepsilon + O(\varepsilon^2) \tag{36}$$

$$\phi(\varepsilon, \nu) = \frac{5(7-\nu)}{24(1-\nu)} + \frac{5(53+\nu)}{126(1-\nu)}\varepsilon + O(\varepsilon^2) \tag{37}$$

where

$$\varepsilon(\nu) \approx \frac{987 - 231\nu - 7\sqrt{10985 + 3878\nu - 3199\nu^2}}{12(139 - 67\nu)} \tag{38}$$

Note that ζ and ϕ, provided up to $O(\varepsilon^2)$, offer sufficient accuracy due to the condition $\varepsilon \ll 1$. In addition, as $\varepsilon \to 0$, these solutions return to those based on the assumption of a spherical cap shape such as in Ref. [16]. In Fig. 2, it can be found that the shape defined in Eq. (32) with $N = 5$ and in Eq. (38) shows excellent agreement with numerics. In the ensuing section, we focus on comparing the prefactors ψ, ζ, ϕ, and $\varphi = \phi^3/\zeta^4$ obtained from solutions I, II, and III with the numerical results.

4 Discussion

4.1 Strain Distributions. Figure 3 shows the equal biaxial strain (rescaled by h^2/a^2) in the center of the pressurized membrane as a function of the Poisson's ratio of the material. The plotted markers are derived from numerical calculations of the nonlinear equilibrium Eqs. (1) and (2) through a finite difference method. We find that Eq. (35), as solution III, demonstrates remarkable agreement with the numerical results, exhibiting an error margin only within 0.16%. Notably, this performance surpasses Hencky's series solution (with an error approximately around 0.31%), which requires solving a lengthy, implicit equation [7,13]. In Fig. 3, the solution by Dai et al. used the spherical cap assumption [16]. The solution by Blundo et al. involved fitting the numerical results, akin to setting $\alpha = 2.2$ in Eq. (22) of solution I (the error is identified to be within 1.9%) [25]. Figure 4 presents a comparison between different analytical solutions and numerical calculations regarding radial and hoop strain distributions. Clearly, solution III, as provided in Eq. (34), continues to exhibit excellent accuracy.

4.2 Pressure–Deflection Relation. Figure 5 illustrates the prefactor governing the cubic pressure–deflection relationship (refer to Eq. (3)) in relation to the Poisson's ratio of the material. We find that the accuracy of all three solutions derived from perturbed spherical cap shapes—expressed in Eqs. (21), (29), and (36), respectively—demonstrates considerable improvement compared to the solution assuming an exact spherical cap shape (as demonstrated in prior works such as Refs. [2,15,16,23]). In particular, the error of solution III, i.e., Eq. (36), remains within 0.5%. This level of accuracy is comparable to Hencky's implicit series solution (at 0.3%) [7,13] and the fitting of numerical results (also at 0.3%), i.e.,

$$\zeta(\nu) \approx (0.7179 - 0.1706\nu - 0.1495\nu^2)^{-3}$$

detailed in Ref. [24]. Note that alternative explicit solutions, including those presented in [2,15,16,23] and the model derived from the fitted $\alpha \approx 2.2$ in [25], exhibit an error of at least 5%.

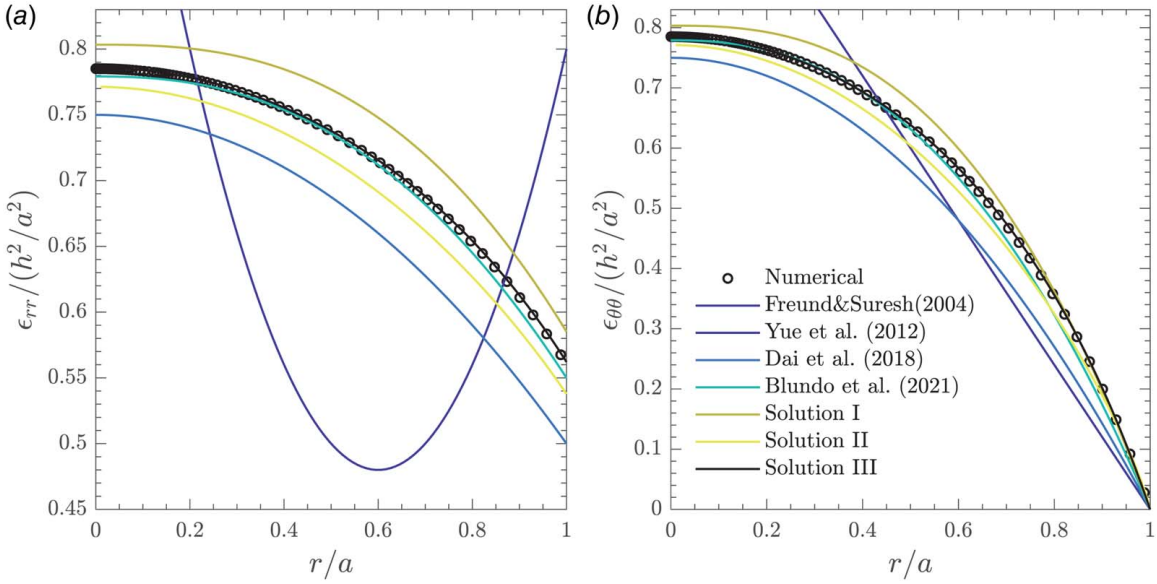

Fig. 4 The rescaled radial (*a*) and hoop (*b*) strain distribution (here, $\nu = 0$). The analytical expressions of solutions I, II, and III are given in Eqs. (18), (27), and (34), respectively. The solution by Dai et al. and Blundo et al. can be found in Refs. [16] and [25], respectively, while the solutions in Refs. [2] and [15] are identical. Here, we used $\nu = 0$ for demonstration. In this case, the maximum ϵ_{rr} occurs at $r = 0$. When $\nu \gtrsim 0.297$, however, the maximum ϵ_{rr} will occur at $r = a$.

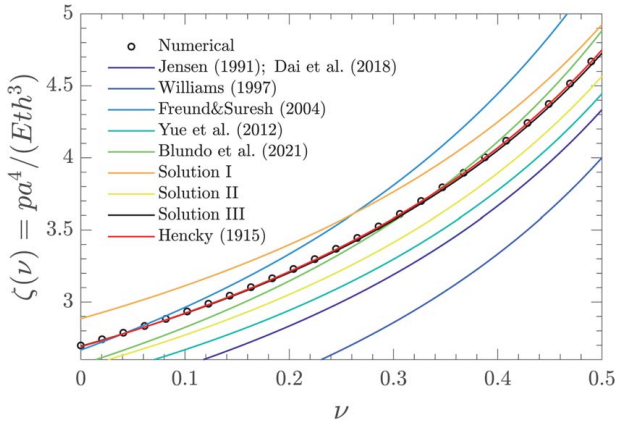

Fig. 5 The prefactor ζ for the cubic pressure–deflection relation as a function of Poisson's ratio. Included are solutions by Jensen [14] (deviation details not published), Dai et al. [16] (assuming a spherical cap shape), Williams [23] (assuming a constant stress), Freund and Suresh [2] (two solutions provided, both assuming a spherical cap shape), Yue et al. [15] (assuming a spherical cap), Blundo et al. [25] (assuming $\alpha \approx 2.2$ in Eq. (21)), and Hencky [7] (the errors in original form is corrected by Fichter [13]). Solutions I, II, and III are given in Eqs. (21), (29), and (36), respectively.

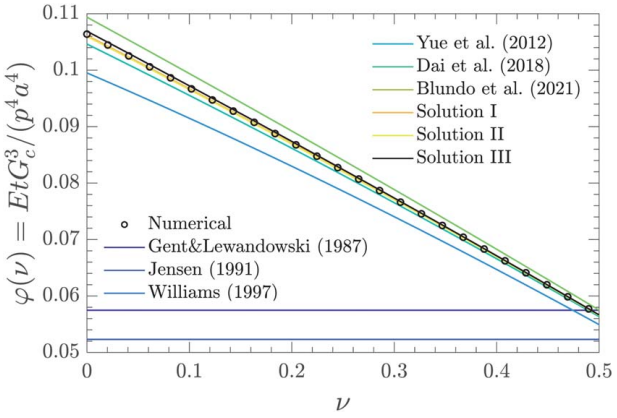

Fig. 7 The prefactor φ in the critical energy release relation in Eq. (6) as a function of Poisson's ratio. The prefactor for $\nu = 0.5$ has been provided by exploiting Hencky's series solution in Refs. [12,14]. Analytical expression for the dependency of φ on Poisson's ratio is given by $\varphi = \phi^3/\zeta^4$, where the dependency of ϕ and ζ on Poisson's ratio has been discussed in Refs. [15,16,25] as well as in our solutions I, II, and III.

4.3 Energy Release Rate. Finally, we discuss our solutions for the scenario of unpinned membrane edges. Figure 6 plots the numerically calculated prefactor for adhesion–aspect ratio relation in Eq. (5) as a function of Poisson's ratio, together with various analytical solutions. Solution III in Eq. (37) upholds its exceptional performance, demonstrating an error of merely 0.7%. By contrast, alternative solutions found in Refs. [15,16,23,25] exhibit errors of at least 6%. Given the prefactors ζ and ϕ, we can investigate the critical blow-up pressure in pressure-controlled blister tests, where a Poisson's ratio dependent prefactor φ emerges as $\varphi = \phi^3/\zeta^4$ (refer to Eq. (6)). In Fig. 7, we have compared various solutions against numerical results concerning φ. In particular, our three sets of solutions exhibit an error of less than 0.5%, while alternative solutions in the literature indicate errors exceeding 2% [12,14–16,23,25]. Note that the solutions provided in Refs. [12,14] are accurate specifically for $\nu = 0.5$.

The blister test solution has garnered significant attention within the literature [22,36]. Apart from the discussions on relations (5) and (6), there have been analytical solutions addressing $\lambda(\nu) = G_c/(p_c h_c)$ in prior studies. By employing Eqs. (3) and (5), we can easily obtain $\lambda = \phi/\zeta$. Further, using solution III (since it has consistent accuracy), we obtain

$$\lambda = \frac{5}{8} + \frac{15}{56}\varepsilon - \frac{15}{56}\varepsilon^2 + O(\varepsilon^3)$$

where $\varepsilon(\nu)$ has been provided in Eq. (38). This has slightly improved accuracy over previous solutions such as $\lambda \equiv 0.65$ in [12], $\lambda \approx 0.651$ only for $\nu = 1/3$ in [14], and $\lambda \equiv 5/8$ in [23] as well as other erroneous solutions such as $\lambda \equiv 1/4$ in [37] and $\lambda = 0.45$ for $\nu = 0.5$ in [38] (due to incorrect energy terms as noted in Ref. [29]).

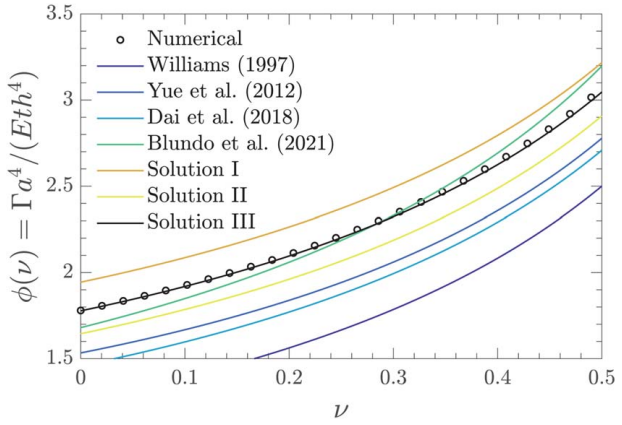

Fig. 6 The prefactor ϕ for adhesion–aspect ratio relation in Eq. (5) as a function of Poisson's ratio. Explicit solutions for this prefactor available in the literature including Refs. [15,16,23,25] are compared to numerical results as well as our solutions I, II, and III expressed in Eqs. (24), (30), and (24), respectively.

5 Concluding Remarks

The analysis given here has focused on improved analytical solutions for the classic problem of pressurized membranes with clamped or adhesive boundary conditions. Three variations of perturbed spherical cap shapes have been tested. We have shown that solution III, based on Eq. (32), exhibited the most significant improvements compared to the other two solutions in terms of strain fields, pressure–deflection relationship, and energy release rate. Remarkably, despite its simplicity, solution III demonstrates unexpected accuracy, rivaling implicit solutions derived through series-based approaches. The idea is similar to our recent perturbation solution to the shaft-loaded elastic membranes [39]. We expect the concept can be extended to address more intricate pressurized/shaft-loaded membrane problems, for instance, by considering additional, practical factors such as residual stresses, nonlinear material behaviors, and the radial component of pressure.

It is important to note that the solutions presented herein are limited to very bendable membranes with moderate rotation (i.e., $h^2/a^2 \ll 1$ and $h \gg t$). While they may find immediate application in ultrathin elastic films such as 2D materials shown in Fig. 1, this analysis overlooks several crucial physical factors pertinent to more generalized thin films. Specifically, the nonlinear elastic response proposed by Eq. (3) tends to linearize under small pressure loads, once accounting for the film's bending rigidity or residual stress [40]. Consequently, the conditions for delamination would exhibit qualitative variations (for an elaborate discussion, refer to [41,42]). Furthermore, the adhesion energy (i.e., the critical strain energy release rate) may vary depending on the specific mode mixity [22,43]. One may anticipate that the influence of bending

rigidity and residual stress on elastic response diminishes as the pressure increases substantially. However, caution is warranted, as fully nonlinear kinematics and material laws may manifest, eluding description by simplistic Föppl membrane theory [31].

Acknowledgment

This research was financially supported by the National Natural Science Foundation of China (12372103) and "The Fundamental Research Funds for Central Universities (Peking University)".

Conflict of Interest

There are no conflicts of interest.

Data Availability Statement

The datasets generated and supporting the findings of this article are obtainable from the corresponding author upon reasonable request.

References

[1] Beams, J., 1959, "Mechanical Properties of Thin Films of Gold and Silver," *Structure and Properties of Thin Films*, John Wiley and Sons, New York, p. 183.
[2] Freund, L. B., and Suresh, S., 2004, *Thin Film Materials: Stress, Defect Formation and Surface Evolution*, Cambridge University Press, Cambridge.
[3] Mansfield, E. H., 1989, *The Bending and Stretching of Plates*, Cambridge University Press, Cambridge.
[4] Dai, Z., Liu, L., and Zhang, Z., 2019, "Strain Engineering of 2D Materials: Issues and Opportunities at the Interface," Adv. Mater., **31**(45), p. 1805417.
[5] Dai, Z., Lu, N., Liechti, K. M., and Huang, R., 2020, "Mechanics at the Interfaces of 2D Materials: Challenges and Opportunities," Curr. Opin. Solid State Mater. Sci., **24**(4), p. 100837.
[6] Dong, W., Dai, Z., Liu, L., and Zhang, Z., 2023, "Toward Clean 2d Materials and Devices: Recent Progress in Transfer and Cleaning Methods," Adv. Mater., p. 2303014.
[7] Hencky, H., 1915, "Uber Den Spannungszustand in Kreisrunden Platten Mit Verschwindender Biegungssteifigkeit," Z. Math. Phys., **63**, pp. 311–317.
[8] Dai, Z., Sanchez, D. A., Brennan, C. J., and Lu, N., 2020, "Radial Buckle Delamination Around 2d Material Tents," J. Mech. Phys. Solids, **137**, p. 103843.
[9] Dai, Z., and Lu, N., 2021, "Poking and Bulging of Suspended Thin Sheets: Slippage, Instabilities, and Metrology," J. Mech. Phys. Solids, **149**, p. 104320.
[10] Dai, Z., Rao, Y., and Lu, N., 2022, "Two-dimensional Crystals on Adhesive Substrates Subjected to Uniform Transverse Pressure," Int. J. Solids Struct., **257**, p. 111829.
[11] Rao, Y., Kim, E., Dai, Z., He, J., Li, Y., and Lu, N., 2023, "Size-Dependent Shape Characteristics of 2d Crystal Blisters," J. Mech. Phys. Solids, **175**, p. 105286.
[12] Gent, A., and Lewandowski, L., 1987, "Blow-Off Pressures for Adhering Layers," J. Appl. Polym. Sci., **33**(5), pp. 1567–1577.
[13] Fichter, W., 1997, "Some Solutions for the Large Deflections of Uniformly Loaded Circular Membranes," NASA Technical Reports. Document ID: 19970023537.
[14] Jensen, H. M., 1991, "The Blister Test for Interface Toughness Measurement," Eng. Fract. Mech., **40**(3), pp. 475–486.
[15] Yue, K., Gao, W., Huang, R., and Liechti, K. M., 2012, "Analytical Methods for the Mechanics of Graphene Bubbles," J. Appl. Phys., **112**(8), p. 083512.
[16] Dai, Z., Hou, Y., Sanchez, D. A., Wang, G., Brennan, C. J., Zhang, Z., Liu, L., and Lu, N., 2018, "Interface-governed Deformation of Nanobubbles and Nanotents Formed by Two-Dimensional Materials," Phys. Rev. Lett., **121**(26), p. 266101.
[17] Blundo, E., Di Giorgio, C., Pettinari, G., Yildirim, T., Felici, M., Lu, Y., Bobba, F., and Polimeni, A., 2020, "Engineered Creation of Periodic Giant, Nonuniform Strains in Mos2 Monolayers," Adv. Mater. Interfaces, **7**(17), p. 2000621.
[18] Wang, G., Dai, Z., Wang, Y., Tan, P., Liu, L., Xu, Z., Wei, Y., Huang, R., and Zhang, Z., 2017, "Measuring Interlayer Shear Stress in Bilayer Graphene," Phys. Rev. Lett., **119**(3), p. 036101.
[19] Wang, P., Gao, W., Cao, Z., Liechti, K. M., and Huang, R., 2013, "Numerical Analysis of Circular Graphene Bubbles," ASME J. Appl. Mech., **80**(4), p. 040905.
[20] Johnson, K. L., Kendall, K., and Roberts, A. D., 1971, "Surface Energy and the Contact of Elastic Solids," Proc. R. Soc. Lond. A, **324**(1558), pp. 301–313.
[21] Griffith, A. A., 1921, "Vi. The Phenomena of Rupture and Flow in Solids," Philos. Trans. Royal Soc. A, **221**(582-893), pp. 163–198.
[22] Liechti, K., 2019, "Characterizing the Interfacial Behavior of 2d Materials: a Review," Exp. Mech., **59**(3), pp. 395–412.
[23] Williams, J., 1997, "Energy Release Rates for the Peeling of Flexible Membranes and the Analysis of Blister Tests," Int. J. Fract., **87**(3), pp. 265–288.
[24] Komaragiri, U., Begley, M., and Simmonds, J., 2005, "The Mechanical Response of Freestanding Circular Elastic Films Under Point and Pressure Loads," ASME J. Appl. Mech., **72**(2), pp. 203–212.
[25] Blundo, E., Yildirim, T., Pettinari, G., and Polimeni, A., 2021, "Experimental Adhesion Energy in Van Der Waals Crystals and Heterostructures From Atomically Thin Bubbles," Phys. Rev. Lett., **127**(4), p. 046101.
[26] Lloyd, D., Liu, X., Christopher, J. W., Cantley, L., Wadehra, A., Kim, B. L., Goldberg, B. B., Swan, A. K., and Bunch, J. S., 2016, "Band Gap Engineering With Ultralarge Biaxial Strains in Suspended Monolayer Mos2," Nano Lett., **16**(9), pp. 5836–5841.
[27] Sanchez, D. A., Dai, Z., and Lu, N., 2021, "2D Material Bubbles: Fabrication, Characterization, and Applications," Trends Chem., **3**(3), pp. 204–217.
[28] Fang, Z., Dai, Z., Wang, B., Tian, Z., Yu, C., Chen, Q., and Wei, X., 2023, "Pull-to-Peel of Two-Dimensional Materials for the Simultaneous Determination of Elasticity and Adhesion," Nano Lett., **23**(2), pp. 742–749.
[29] Wan, K.-T., and Mai, Y.-W., 1995, "Fracture Mechanics of a New Blister Test With Stable Crack Growth," Acta Metall. Mater., **43**(11), pp. 4109–4115.
[30] Koenig, S. P., Boddeti, N. G., Dunn, M. L., and Bunch, J. S., 2011, "Ultrastrong Adhesion of Graphene Membranes," Nat. Nanotechnol., **6**(9), pp. 543–546.
[31] Rao, Y., Qiao, S., Dai, Z., and Lu, N., 2021, "Elastic Wetting: Substrate-Supported Droplets Confined by Soft Elastic Membranes," J. Mech. Phys. Solids, **151**, p. 104399.
[32] Wan, K.-T., and Lim, S.-C., 1998, "The Bending to Stretching Transition of a Pressurized Blister Test," Int. J. Fracture, **92**(4), pp. 43–47.
[33] Sanchez, D. A., Dai, Z., Wang, P., Cantu-Chavez, A., Brennan, C. J., Huang, R., and Lu, N., 2018, "Mechanics of Spontaneously Formed Nanoblisters Trapped by Transferred 2d Crystals," Proc. Natl Acad. Sci. USA, **115**(31), pp. 7884–7889.
[34] Boddeti, N. G., Koenig, S. P., Long, R., Xiao, J., Bunch, J. S., and Dunn, M. L., 2013, "Mechanics of Adhered, Pressurized Graphene Blisters," ASME J. Appl. Mech., **80**(4), p. 040909.
[35] Yu, C., and Dai, Z., 2023, "Characterizing the Wetting Behavior of 2d Materials: A Review," J. Mater. Inf., **3**(3), p. 20.
[36] Cao, Z., Tao, L., Akinwande, D., Huang, R., and Liechti, K. M., 2016, "Mixed-Mode Traction-Separation Relations Between Graphene and Copper by Blister Tests," Int. J. Solids Struct., **84**, pp. 147–159.
[37] Hinkley, J., 1983, "A Blister Test for Adhesion of Polymer Films to SiO2," J. Adhesion, **16**(2), pp. 115–125.
[38] Briscoe, B., and Panesar, S., 1991, "The Application of the Blister Test to an Elastomeric Adhesive," Proc. R. Soc. A, **433**(1887), pp. 23–43.
[39] Chen, E., and Dai, Z., 2023, "Axisymmetric Peeling of Thin Elastic Films: A Perturbation Solution," ASME J. Appl. Mech., **90**(10), p. 101011.
[40] Wan, K.-T., Guo, S., and Dillard, D. A., 2003, "A Theoretical and Numerical Study of a Thin Clamped Circular Film Under an External Load in the Presence of a Tensile Residual Stress," Thin. Solid. Films., **425**(1–2), pp. 150–162.
[41] Cotterell, B., and Chen, Z., 1997, "The Blister Test–Transition From Plate to Membrane Behaviour for an Elastic Material," Int. J. Fracture, **86**(3), pp. 191–198.
[42] Arjun, A., and Wan, K.-T., 2005, "Derivation of the Strain Energy Release Rate G From First Principles for the Pressurized Blister Test," Int. J. Adhes. Adhes., **25**(1), pp. 13–18.
[43] Jensen, H. M., 1998, "Analysis of Mode Mixity in Blister Tests," Int. J. Fracture, **94**(1), pp. 79–88.